Biomaterials and Biosystems 8 (2022) 100065

Contents lists available at ScienceDirect

Biomaterials and Biosystems

journal homepage: www.elsevier.com/locate/bbiosy

A quest for cytocompatible metal organic frameworks in non-viral gene therapy: Relevance of zeolitic imidazolate framework-8

A. Poddar[a,b,c], S. Pyreddy[a,b], S.A. Polash[a,b], C.M. Doherty[c], R. Shukla[a,b,*]

[a] Ian Potter NanoBiosensing Facility, NanoBiotechnology Research Laboratory (NBRL), School of Science, RMIT University, Melbourne, Victoria 3001, Australia
[b] Centre for Advanced Materials and Industrial Chemistry, School of Science, RMIT University, Melbourne, Victoria 3001, Australia
[c] CSIRO Manufacturing, Clayton, Victoria 3168, Australia

ARTICLE INFO

Keywords:
MOF
ZIF
UiO
MIL
Gene

ABSTRACT

Metal-organic frameworks (MOFs) are an emerging group of nanomaterials for successful biomedical applications in gene therapy. The most commonly biocompatible MOFs are zinc-based ZIFs, zirconium-based UiOs, and iron-based MILs. However, despite increasing applications, a comparative study to underscore the critical factors for determining effective gene delivery by such MOFs is lacking. Herein, we evaluate the potential of UiO-66 and MIL-88B and ZIF-8 for gene therapeutics delivery; revealing the comparative importance of ZIF-8. Cytotoxicity assays proved insufficient for selecting the ideal gene delivery MOF vehicle. Synthesis conditions such as ability of the MOF scaffold to envelop the gene during in-situ synthesis, post-treatment such as washing, and gene loading efficiency proved to be the critical factors in determining the favourable MOF from the material selection perspective. Rapid in-situ synthesis under physiological conditions, successful gene loading, and low concentration requirements favour ZIF MOFs as gene delivery vehicles. Impact on cellular physiology, metabolism, and architecture revealed neutrality of the delivery system; and relative effects on pro-inflammatory and anti-inflammatory cytokines suggest immunomodulatory impact.

1. Introduction

Metal-organic frameworks (MOFs), materials built from metal ions and organic ligands [1], are promising nanoplatforms for drug/biomolecule delivery [2]. They have been used for drug and siRNA delivery, chemodynamic therapy for cancer, encapsulation of polysaccharides, proteins, nucleic acids and prokaryotic as well as eukaryotic cells [3,4]. The most successful MOFs for biological applications are the Zr-based Universitetet i Oslo (UiO) series [5], Fe-based Materials of Institute Lavoisier (MIL) series [6] and the biomimetically mineralised Zn-based Zeolitic Imidazolate Framework (ZIF) series [7]. UiO MOFs have been used to deliver drugs and small nucleic acids like siRNAs to cancer cells in vitro [8,9]. MILs are reported to be non-toxic, biodegradable nanocarriers suitable for antitumoral and retroviral drug delivery, imaging, and minimal in vivo toxicity [10,11]. ZIFs have been reported for drug and biomolecule delivery with demonstrated biocompatibility, biodegradability, protection, and encapsulation properties [12–16]. The most current bio-application of MOFs is in the field of gene therapy. It is a therapeutic option whereby the correct form of a malfunctioning gene is delivered into a dysregulated cell with the help of a carrier called a 'vector' [17]. As DNA-MOF complexes have been modelled in reported studies, MOFs are being investigated as gene therapy vectors. For instance, ZIF-8 and amine-synthesised UiO-66 along with CpG oligonucleotides have been used for studying DNA-MOF interactions [18]. Oligonucleotides have also been loaded onto Zr and Fe-based MOFs [19]. However, most of the reports utilized short-chain DNA sequences which are significantly different from functional genes suitable for gene therapy. To the best of our knowledge, successful gene therapy utilizing functional genes has only recently been reported with ZIF-8 based MOFs [20–22].

Multiple studies demonstrate the biological usefulness of UiOs, MILs, and ZIFs with varying degrees of efficiency, yet the application of all three in gene therapy is lacking. Moreover, the impact of such novel gene delivery on the basal cellular functions of host cells remains unknown. Analysis of the underlying cellular infrastructure as maintained by the network of housekeeping proteins is essential for calibrating the downstream effect of MOFs on genomic expression. Measuring immunotoxicity of the MOFs is further critical for determining the immune- or inflammatory response. The potential immunotoxicity induced by these MOFs along with their ability to interact by either enhancement or suppression of the immune system remains largely unknown. Herein, UiO-66, MIL-88B and ZIF-8 are evaluated for gene delivery by assessing their efficiency to load intact genes. Our results indicate the ease of use of ZIF-8 for gene loading and outline the shortcomings that need

* Corresponding author.
E-mail address: ravi.shukla@rmit.edu.au (R. Shukla).

https://doi.org/10.1016/j.bbiosy.2022.100065
Received 1 June 2022; Received in revised form 8 August 2022; Accepted 4 October 2022

to be addressed if gene therapy is to be carried out successfully using nano MOFs. Furthermore, the effect of housekeeping genes on cellular physiology, metabolism, and homoeostasis is evaluated by quantifying the mRNA expression of glyceraldehyde-3-phosphate dehydrogenase (GAPDH) and beta-actin (β-ACTIN), as well as non-housekeeping ribosomal protein SA (RPSA) genes. GAPDH catalyses multiple cell reactions and is heavily involved in physiology, cytoskeleton plasticity and several other processes [23,24]. β-ACTIN forms the cytoskeleton with tremendous roles in normal maintenance such as cell migration and cell division [25,26]. RPSA is an essential component of basement membranes and is involved in multiple physiological as well as pathological processes [27]. In addition to cell signalling and growth, it is overexpressed in aggressive tumours and acts as a receptor for prions, viruses, and bacteria [28]. While traditionally considered as constitutive genes without any supposed fluctuations in expression, both GAPDH and β-ACTIN expressions have been known to vary significantly under foreign and stressful conditions, resulting in deviations in the physiological machinery [24,29]. RPSA, on the other hand, is specifically upregulated in cancer and has been targeted using MOF-based gene delivery carrying RPSA-specific genes [22]. However, the impact on basal RPSA utilizing a non-targeting MOF system is yet unknown. In the study, we evaluate the expressions of GAPDH, β-ACTIN, and RPSA upon using a MOF-based delivery system. We report no significant deviation, signifying the lack of cellular stress caused by the delivery system itself.

Finally, the impact on cell immunity is evaluated. The introduction of foreign materials to the natural cellular environment forms the basis for triggering the immune response carried out by the release of cytokines. Cytokines are pleiotropic, well known to indicate immunotoxicity and can be either pro-inflammatory or anti-inflammatory, with synergistic as well as antagonistic activities [30]. The immunomodulatory impact of the MOF-based delivery system on the pro-inflammatory cytokine IL8 and anti-inflammatory cytokine is assessed. IL8 is a pro-inflammatory chemotactic cytokine playing a major role in acquired immune responses by triggering inflammation through neutrophil migration, mononuclear phagocytes, and mast cells [31]. Conversely, IL10 is a potent inflammation suppressing cytokine that inhibits interferon-γ production and antigen-specific T-cell activation [32]. The balance between pro- (IL8) and anti-inflammatory (IL10) cytokines plays a fundamental role in determining the degree of immune response [33]. We report a significant suppression of the pro-inflammatory cytokine IL8 and no significant dysregulation of the anti-inflammatory cytokine IL10 upon interaction with the MOF delivery system. Based on our results, the lack of enhanced activation indicates the non-immunotoxic nature of these MOFs.

In brief, we find ZIF-8 to be the most facile and rapid to synthesize MOF for gene loading, as compared to UiO-66 and MIL-88B; with room temperature and aqueous conditions that allow for one-step gene loading during MOF synthesis itself, indicating the ZIF-8 scaffold forms around the gene. More than 80% gene loading was observed, with ZIF-8 concentrations well below 1 μg/ml. No significant difference in housekeeping gene expression GAPDH and β-ACTIN or RPSA was seen with gene@ZIF-8, along with suppression of pro-inflammatory cytokine IL8 and no significant changes to anti-inflammatory cytokine IL10; indicating a neutral delivery system and minimal immunotoxicity. Taken together, these results shed light on the viability of ZIF-8 for gene delivery and important considerations for MOF-based gene therapy.

2. Materials and methods

2.1. Materials

Zinc acetate dihydrate ($Zn(OAc)_2{\cdot}2H_2O$), 2-Methylimidazole (2mIM), ethanol, zirconium chloride ($ZrCl_4$), terephthalic acid, benzoic acid, hydrochloric acid (HCl), dimethylformamide (DMF), 2-aminoterephthalic acid, iron(III) chloride hexahydrate ($FeCl_3{\cdot}6H_2O$), glacial acetic acid, Tris-base, ethylenediaminetetraacetic acid disodium salt (EDTA), ultra-pure grade nitric acid were purchased from Sigma-Aldrich. PC3 prostate cancer cells were kindly provided by Prof John Mariadoson's lab in the Olivia Newton-John Cancer Research Centre. The DNA plasmid, pCDNA5frt-EGFP-N1(CAT), was kindly provided by Prof. Peter Smooker at RMIT University [20]. Cell culture flasks, 6-, 24- and 96- well plates. 3-(4,5-dimethylthiazol-2-yl)-2,5-diphenyltetrazolium bromide (MTT), dimethyl sulfoxide (DMSO), DNase/RNase free water, Roswell Park Memorial Institute (RPMI) medium [supplemented with 4.5 g/L D-glucose, 25 mM HEPES, 0.11 g/L sodium pyruvate, 1.5 g/L sodium bicarbonate, 2 mM L-glutamine, 10% fetal bovine serum (FBS), and 1% penicillin-streptomycin], agarose and SyberSafe DNA stain were purchased from Thermo Fisher Scientific.

2.2. Methods

2.2.1. Synthesis of UiO-66

The synthesis of UiO-66 was based on the method described by Zhu et al [9]. $ZrCl_4$ (466 mg, 2 mmol), terephthalic acid (320 mg, 2 mmol), benzoic acid (2.44 g, 20 mmol), and HCl (37%, 12 M; 0.33 mL, 4 mmol) in 36 mL of DMF were ultrasonically dissolved in a vial. The mixture was heated in a heat block at 120 °C for 48 hours. After cooling down to room temperature, a white powder of UiO-66 was harvested by centrifugation at 5000 rpm for 10 minutes. The supernatant was discarded, and the pellet, containing the polycrystalline powder, was washed 3 times with DMF at room temperature.

2.2.2. Synthesis of MIL-88b

Synthesis of the terephthalate -Fe-based MOF was based on the method described by Liu et al [11]. Terephthalic acid (0.115 g, 0.692 mmol) and $FeCl_3{\cdot}6H_2O$ (0.187 g, 0.692 mmol) were dissolved in 15 mL of DMF. Acetic acid (3.45) mmol was subsequently added to the reaction solution. The solution was then placed in a heat block at 120 °C for 4 hours for crystallization. After cooling to room temperature, the particles were collected by centrifugation at 5000 rpm for 10 minutes. The supernatant was discarded, and the pellet, containing the polycrystalline powder, was washed 3 times with DMF and ethanol.

2.2.3. Synthesis of ZIF-8

The synthesis of ZIF-8 was based on the method described by Hoop et al [13]. $Zn(OAc)_2{\cdot}2H_2O$ (0.3 g) was dissolved in 5 mL of deionized (DI) water and added to a solution of 2mIM (1.12 g) in 5 mL of DI water. The mixture was stirred at room temperature till it turned cloudy and incubated at room temperature for 10 minutes. The solution was centrifuged at 5000 rpm for 10 minutes to stop the reaction. The supernatant was discarded, and the pellet, containing the polycrystalline powder, was washed 3 times with ethanol.

For assessing the gene loading potential of the three MOFs, a plasmid expressing green fluorescent protein (plGFP) was selected as the representative gene. A plasmid is a DNA molecule that carries intact genes on its sequences and can be expressed in mammalian cells following transfection [34,35]. The amount of plGFP to be used for synthesis was selected based on the optimal amount of DNA required for transfection. For the transfection of epithelial cells such as PC3 cells in a 24-well plate, with a surface area of 1.9 cm^2 using plasmid GFP, 250–500 ng DNA is reported to be an optimal amount [36]. Hence, this quantity was used for loading the genes onto the MOFs to synthesize gene@MOF bioconjugates viz. gene@ZIF-8, gene@UiO-66, and gene@MIL-88B

2.2.4. Synthesis of gene@UiO-66

Following the protocol outlined in 2.2.1, UiO-66 was synthesized. In a 1.5 ml tube, 1 μl 0.34 pM plGFP (500 ng) was incubated with 10 μl of the UiO-66 (25 μg/ml) for 30 mins which is the reported time required for loading of other nucleic acid molecules onto UiO-66 [8]. After loading, the MOFs were centrifuged at 10,000 rcf for 15 min. The supernatant was kept aside for agarose gel electrophoresis and the pellet of UiO-66 was collected, washed, and re-suspended in an aqueous solution.

2.2.5. Synthesis of gene@MIL-88B

A 10 μl of MIL-88B (25 μg/ml) was synthesized as above and incubated with 0.34 pM plGFP (500 ng) for 30 mins. After incubation, the gene-loaded MIL-88B was centrifuged at 10,000 rcf for 15 min. The supernatant was kept aside for agarose gel electrophoresis and the precipitate of MIL-88B was collected, washed, and re-suspended in aqueous solutions.

2.2.6. Synthesis of gene@ZIF-8

Following the protocol outlined above, ZIF-8 proved to be the only MOF particle that allowed for synthesis and gene loading in a one-step process during synthesis rather than post-synthesis. In a 1.5 ml tube, 1 μl of 0.34 pM plGFP (500 ng) was added to aqueous solutions of 160 mM 2mIM (10 μl) followed by the addition of a 40 mM $Zn(OAc)_2{\cdot}2H_2O$ (10 μl) precursors at room temperature. The clear solution becomes cloudy and turbid within 10–15 seconds, and following incubation of 10 minutes, the solution was centrifuged at 10,000 rcf for 10 minutes. The supernatant was kept aside for agarose gel electrophoresis and the pellet was collected and washed in ethanol or water for gene@ZIF-8. The re-suspended aqueous solutions were used for further characterizations and cellular uptake.

2.2.7. X-ray diffraction (XRD)

XRD measurements were performed using a Bruker D8 Discover General Area Detector Diffraction System (GADDS) Diffractometer. The XRD beam monochromator was a copper target x-ray tube with Cu Kα radius 1.544 Å, set to 40 kV generator intensity and 40 mA generator current. Minimal sample preparation steps were required for analysis. The samples were mounted on sample holder stubs and placed into the instrument. All spectra were collected at room temperature. The step size was 0.01° and the collection range (2θ) was set from 5° to 70° Data was collected in raw file form (.raw) and converted to UXD file format using the File Exchange Program XCH (Ver. 5.0.10, 2004, Bruker AXS, Socabim, Karlsruhe, Germany) before data analysis. For analysis, the collected spectra were plotted using the OriginPro software from OriginLab [37]. The application of XRD was used to verify the MOFs synthesized by comparing the experimentally synthesised MOF diffraction spectra to that of simulated x-ray diffraction spectra patterns for the established MOF crystal structures deposited in the CCD and COD.

2.2.8. Scanning electron microscopy (SEM)

SEM was performed using a Carl Zeiss Gemini Field Emission Scanning Electron Microscope. Following synthesis of the MOFs, approximately 2 μl of the synthesized sample mixture was drop cast to a silicon wafer and allowed to air dry. This was followed by sputter coating with 5–6 nm of iridium. Imaging was done under high-resolution visualization at EHT 5.0 kV with High Efficiency (HE-SE2) detector for collecting secondary electrons.

Octahedral to rounded crystals were observed for UiO-66, tetrahedral-like morphology was observed for MIL-88B and rhombic dodecahedral particles were observed for ZIF-8. The morphologies observed matched with those reported in the literature for UiO-66 [38], MIL-88B [39], and ZIF-8 [40].

2.2.9. Fourier transformed infra-red (FTIR) spectroscopy

FTIR was carried out using a Perkin Elmer Spectrum 100 instrument with a Spotlight 400 attachment. Potassium bromide (KBr) was added to the synthesized MOF pellet. This mixture was kept at 60–70 °C for 1–2 hours to get rid of moisture. The KBr and MOF pellet was mixed thoroughly and transferred to the instrument sample holder. Before the sample run, pure KBr was run as background. The average spectra of 128 scans collected from 4000–400 cm^{-1} range with 2 cm^{-1} resolution.

2.2.10. Cytotoxicity

PC3 cells were maintained in RPMI medium supplemented with 4.5 g/L D-glucose, 25 mM HEPES, 0.11 g/L sodium pyruvate, 1.5 g/L sodium bicarbonate, 2 mM L-glutamine, 10% FBS, and antibiotics. PC3 cells were seeded in 96 well plates with a density of 1000 cells/well and incubated at 37 °C with 5% CO_2 overnight. The next day, treatments were prepared by resuspending the synthesized MOFs in 1 ml MilliQ water each. Cells were then treated with 12.5, 25, 50, and 100 μg/ml of ZIF-8, UiO-66, and MIL-88B After 24 hours, the treatment media was aspirated from respective wells, and 100 μL of serum-free medium containing 0.5 mg/mL of MTT was added to each well and incubated for 4 hours in dark at 37 °C. After incubation, the medium containing MTT was replaced with DMSO for the dissolution of the purple formazan crystals. The absorbance was measured in a microplate reader at 570 nm with a reference wavelength of 630 nm. The percentage cell viability is calculated by the formula [(absorbance of treated cells/absorbance of untreated cells) *100]. Pristine or untreated cells (UNT) that did not receive any treatment were used as controls. The data was represented based on duplicates of duplicate independent experiments. Significant differences were determined by two-way ANOVA on GraphPad Prism. The level of statistical significance was $^{**}p < 0.001$ and $^{****}p < 0.0001$.

2.2.11. Cellular transfection

PC3 cells were maintained in RPMI medium supplemented with 4.5 g/L D-glucose, 25 mM HEPES, 0.11 g/L sodium pyruvate, 1.5 g/L sodium bicarbonate, 2 mM L-glutamine, 10% FBS, and antibiotics. Approximately 50,000 cells/well were seeded in a 24-well plate and incubated in humidified 5% CO_2 37 °C incubators. Cells were grown to 40–50% confluency and transfected with plGFP using Lipofectamine 3000 reagent (Thermo Fischer) following manufacturer's protocol or plGFP@ZIF-8. Untreated cells were used as control. The transfection media was replaced with fresh media at 3 hours post-treatment. Incubation was carried out in humidified 5% CO_2 37 °C incubators for up to 96 hours. Cells were then fixed with 4% paraformaldehyde, stained with Hoechst nuclear stain, and imaged in a fluorescence microscope. Water-washed plGFP@ZIF-8 was used for transfections.

2.2.12. Agarose gel electrophoresis

A 1% (w/v) agarose gel was prepared by adding 1 g agarose in 100 ml 1xTAE buffer and heating till the solution was completely clear. 1xTAE was prepared from a stock of 50xTAE made by dissolving 242 g Tris-base, 57.1 mL glacial acetic acid, and 100 mL 0.5 M EDTA (pH 8.0) solution, and bringing the final volume up to 1 L. The solution was cooled to roughly 50 °C and a SyberSafe DNA stain was added. The gel was poured into the casting tray with the comb in place. After gel polymerized, the comb was removed to expose sample wells and the gel was placed into the tank of the electrophoresis apparatus. 1xTAE was poured to cover the gel and to act as a running buffer. The gel was run with the following samples with voltage at 100 V for 1 hour: pure plGFP (control) and supernatants of the gene loading reaction mixtures of UiO-66, MIL-88B, and ZIF-8. After run completion, the DNA bands were visualized by placing the gel under a UV light source in a Gel Doc system.

The DNA bands obtained in the gel image were quantitated using FIJI [41]. In FIJI, the LUTs were inverted and the regions of interest were isolated using the rectangle tool. The band intensity peaks were graphed and the area under the curve of each peak was calculated. The peak percentage of each experimental band (lanes with supernatants of gene@MOF) was divided by the peak percentage of the control band (pure plGFP) to give the relative percent of DNA quantity associated with the gene@MOF composites.

2.2.13. Inductively coupled plasma – mass spectrometer (ICP-MS)

The MOF pellet of gene@ZIF-8 synthesized was of insufficient quantity to determine concentration by vacuum drying of samples. Hence, verification of the ZIF-8 amount associated with the synthesis of gene@ZIF-8 using varying gene concentrations (0.25, 0.5, 1, and 2 μg/ml) was carried out using ICP-MS by determining the zinc (Zn^{2+}) concentration. The concentration of gene@ZIF-8 was calculated based

on the Zn^{2+} ions present in the MOF particles as described by Zahmakiran et al [42] with some modifications. Briefly, the prepared gene@ZIF-8 was acid digested in 0.2 mL of ultra-pure grade 70% HNO_3 on a heating block at 105 °C for 4 hours. The digested sample was diluted with MilliQ water and acidified to 2% HNO_3. The Zn^{2+} ion concentration was then measured with ICP-MS (7700X, Agilent Technologies). The percentages of soluble Zn^{2+} obtained were used to determine the ZIF-8 concentration in gene@ZIF-8 suspensions [43].

2.2.14. Quantitative RT-PCR

Total RNA was extracted from control untreated and experimental treated cells using guanidinium phenol reagent (TRIzol reagent; Invitrogen) following manufacturer's protocol. The RNA pellet obtained was dissolved in 30 µl DEPC water and purity and concentration were quantified using OPTIZEN NanoQ. Reverse transcription was immediately carried out on 2 µg RNA from each sample using a High-Capacity cDNA Reverse Transcription Kit (ThermoFisher) following the manufacturer's protocol. The reaction was conducted in a T100™ Thermal Cycler (Bio-Rad) with the following step details for a 20 µl reaction volume: 25 °C (10 mins), 37 °C (2 hours), 85 °C (5 mins) and 4 °C (hold).

For real-time quantitative evaluation of β-ACTIN, GAPDH, RPSA, IL8, and IL10, qPCR was carried out on the cDNA with specific qPCR primers. The TaqMan™ Fast Universal PCR Master Mix (2X), no AmpErase™ UNG (ThermoFisher) was used with TaqMan™ Gene Expression Assay (FAM) ID Hs01060665_g1 (for β-ACTIN), Hs02786624_g1 (for GAPDH), and Hs03046712_g1 (for RPSA). Manufacturer's protocol was followed, and the reaction was conducted in a 7500 Fast Real-Time PCR System (Applied Biosystems) with the following cycle specifications for a 10 µl reaction volume: 95 °C (20 sec), [95 °C (3 sec), 60 °C (30 sec)] x40 cycles and 4 °C (hold).

The CT values obtained were normalized to untreated cells. The "fold-over untreated" method was used to calculate the expression level in treated samples as compared to untreated samples [44].

3. Results

3.1. Synthesis and characterisations of UiO-66, MIL-88b and ZIF-8 without and with plGFP gene loading

Synthesis of UiO-66, MIL-88B and ZIF-8 MOFs was carried out as described in Section 2. UiO-66 precursors were added to DMF along with benzoic acid and hydrochloric acid and heated at 120 °C for 48 hours. MIL-88B precursors were added to DMF along with acetic acid and heated at 120 °C for 4 hours. UiO-66 and MIL-88B were harvested after cooling down, centrifugation, and washing with DMF. For ZIF-8, precursors were dissolved in deionized water at room temperature and incubated for 10 minutes. ZIF-8 was obtained following centrifugation and washing with ethanol. XRD was used for structural verification of the synthesized MOFs (Fig. 1A-C). SEM was used to visualise morphology (Fig. 1D-F). Octahedral to rounded crystals were observed for UiO-66, tetrahedral like morphologies were observed for MIL-88B and rhombic dodecahedral particles were observed for ZIF-8. FTIR and UV–vis absorbence spectroscopy further verified the synthesized MOFs where the spectra were in good agreement with reported spectra (Fig. 1G-I and S1).

3.2. Cytotoxicity

For evaluating cytotoxicity, studies using the MTT assay were carried out to determine effects on cell viability. The results from this study demonstrated that increasing MOF concentrations lead to progressive decline in viability (Fig. 2). Up to a concentration of 25 µg/ml, no significant toxicity was observed for any of the three MOFs. Results indicated that MIL-88B was slightly less toxic at 50 µg/ml than ZIF-8 or UiO-66. At the highest concentration of 100 µg/ml, MIL-88B showed mean viability of 77%, with ZIF-8 and UiO-66 giving slightly less mean viabilities of 61% and 65%. Up to 25 µg/ml, viability was above 80% for all. Below 50 µg/ml, good viability was seen with the three MOFs, while at 100 µg/ml, the MOFs significantly reduced cell viability to a similar extent.

3.3. Gene loading potential of UiO-66, MIL-88b and ZIF-8

Gene loading potential was investigated using a 6549 basepair plasmid expressing (plGFP) for loading with the MOFs: gene@UiO-66, gene@MIL-88B and gene@ZIF-8 (Fig. 3A). Gene loading was quantified by resolving supernatants of gene@MOF synthesis mixtures on agarose gel electrophoresis. DNA bands were visualized by placing the gel under a UV light source in a Gel Doc system (Fig. 3B). DNA band was visible for pure plGFP control DNA sample, which was used to quantify DNA amount based on band intensity. Bands were also clearly visible with the same intensity as that of control DNA for the supernatants of UiO-66 and MIL-88B However, the supernatant of ZIF-8 showed a very faint DNA band as compared to the control. On quantification by normalising to control DNA, clear bands with ca. 89% and 91% DNA were present with supernatants of UiO-66 and MIL-88B, respectively. The supernatant of ZIF-8 showed a very faint band with ca. 11% DNA. Thus, in the cases of gene@UiO-66 and gene@MIL-88B, most of the loaded plGFP remained unreacted in the supernatant; with only ca. 10% gene loaded onto the respective MOF pellets. Whereas for gene@ZIF-8, ca. 11% of the loaded plGFP remained with the supernatant. A further notable observation from the agarose image is that the supernatants of MIL-88B and UiO-66 show smeared bands of DNA while the supernatant of ZIF-8 does not.

3.4. Evaluation and visualisation of gene loading in gene@ZIF-8

ZIF-8 quantity associated with gene@ZIF-8 was evaluated using ICP-MS, for the range of gene concentrations required for bioactivity (Fig. 3C). The highest amount of gene@ZIF-8, as calculated from Zn^{2+} concentration, was found to be 0.65 µg/ml when synthesized with 1 µg/µl plGFP, corresponding to a calculated value of roughly 4×10^{13} Zn atoms/ molecule of the plasmid. Morphological impact was assessed by in vitro transfection, SEM and fluorescence imaging of cells treated with the water washed particles of gene@ZIF-8 (Fig. 4A-B). Cells treated with plGFP@ZIF-8, using 1 µg/µl plGFP, retained similar morphology as untreated control cells, as can be seen from the SEM images (Fig. 4A). The red arrows indicate the presence of plGFP@ZIF-8 on the cell surface at 3 hours of treatment. Gene expression of plGFP could be gradually visualized as (GFP) 96 hours post treatment under a fluorescence microscope (Fig. 4B). Cells treated with plGFP@UiO-66 or plGFP@MIL-88B retained cellular morphology similar to control but did not show any green fluorescence (Fig. S2).

3.5. Impact of gene@ZIF-8 on constitutive gene expression

In order to evaluate the effect on endogenous physiology, gene expression levels of two housekeeping markers (β-ACTIN and GAPDH), and a cancer metabolic marker RPSA was quantitated using RT-PCR (Fig. 4C). Following in vitro treatment with plGFP@ZIF-8, RNA of PC3 cells was extracted from treated and untreated control cells. Quantitative RT-PCR with β-ACTIN, GAPDH and RPSA-specific primers revealed the changes in fold expression as compared to untreated cells. No significant difference in the expression levels was obtained. As seen from the PCR results, the ZIF-based MOF delivery system does not disrupt the major biochemical pathways of β-ACTIN, GAPDH and RPSA expressions.

3.6. Immunomodulatory impact of gene@ZIF-8

Gene expression levels of anti- and proinflammatory cytokines IL10 and IL8, respectively, were quantitated using RT-PCR. Following in vitro treatment with plGFP@ZIF-8, RNA of PC3 cells was extracted from

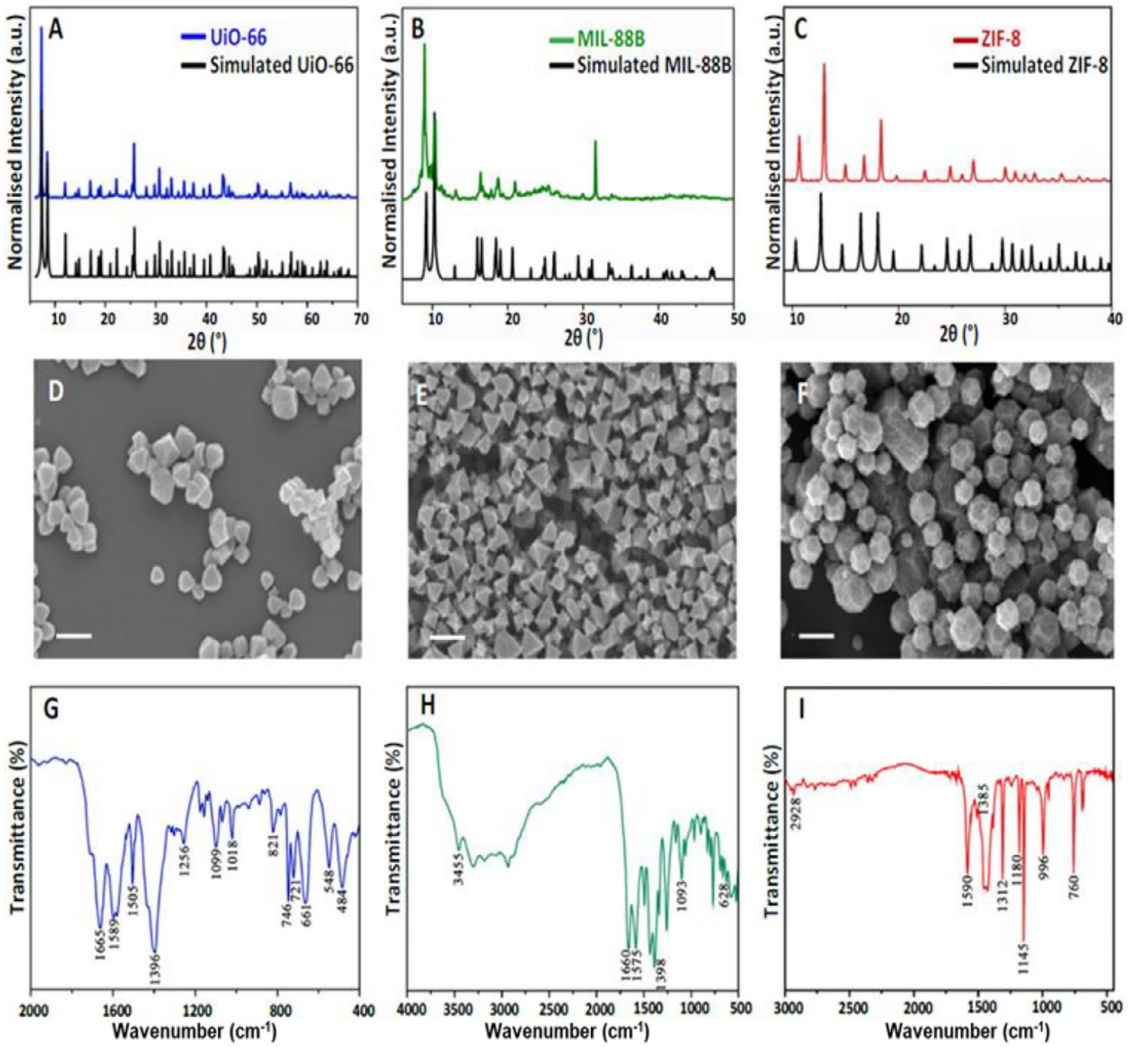

Fig. 1. XRD patterns of (A) synthesized UiO-66 compared to simulated UiO-66, (B) synthesized MIL-88B compared to simulated MIL-88B, and (C) synthesized ZIF-8 compared to simulated ZIF-8. SEM images of (D) UiO-66, (E) MIL-88B, and (F) ZIF-8; scale bars correspond to 0.2 μm. FTIR spectra of (G) UiO-66, (H) MIL-88B, and (I) ZIF-8 [N=3 for each].

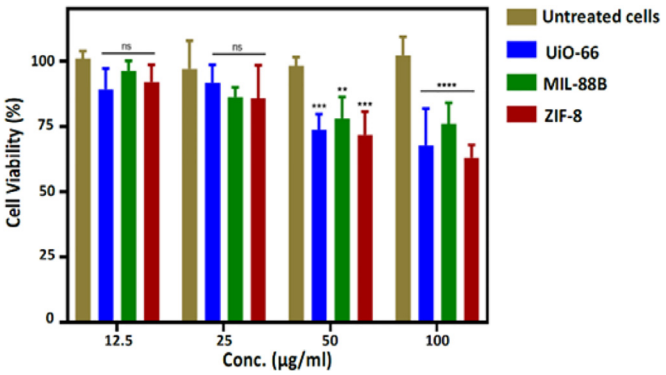

Fig. 2. Effect of UiO-66, MIL-88B and ZIF-8 on cell viability. MOFs are non-toxic up to 25 μg/ml. Data shown for three independent experiments [N=3]. $^{**}p < 0.001$, $^{***}p < 0.0002$, $^{****}p < 0.0001$, ns – not significant.

treated and untreated control cells. Significantly, no over-expression of the cytokines was seen. Moreover, there is a significant suppression of the inflammation promoting cytokine IL8 by ca. 30% as compared to untreated cells. IL8 attracts and activates neutrophils, the "first cellular line of defence" to inflammatory regions. Reduction in IL8 expression indicates suppression of inflammation as a result of the MOF delivery system along with the nature of immunostimulation/immunotoxicity. The anti-inflammatory cytokine IL10 expression undergoes no significant changes. In addition to the non-cytotoxic results obtained and the lack of observed changes to basal constitutive cellular architecture, neutral immunomodulatory effect of gene@ZIF-8 is thus indicated.

4. Discussions

4.1. Synthesis and characterisations of MOFs and gene@MOFs

UiO-66, MIL-88B and ZIF-8 MOFs were synthesized based on the methods described by Zhu et al [9], Liu et al [11], and Hoop et al [13], respectively. Comparable to previous reports [38–40], UiO-66 possessed octahedral to rounded particles, MIL-88B had tetrahedral-like morphologies and ZIF-8 was found to have rhombic dodecahedral particles. Experimental spectra were in good agreement with that of simulated XRD spectra collected from the Cambridge Structural Database (CSD) and Crystallography Open Database (COD) for UiO-66, MIL-88B and ZIF-8. For UiO-66, a comparison was done with simulated UiO-66 powder XRD spectrum with CSD details including RUBTAK03, Deposition Number 1,018,045; COD: Information card entry 4,512,072 [45].

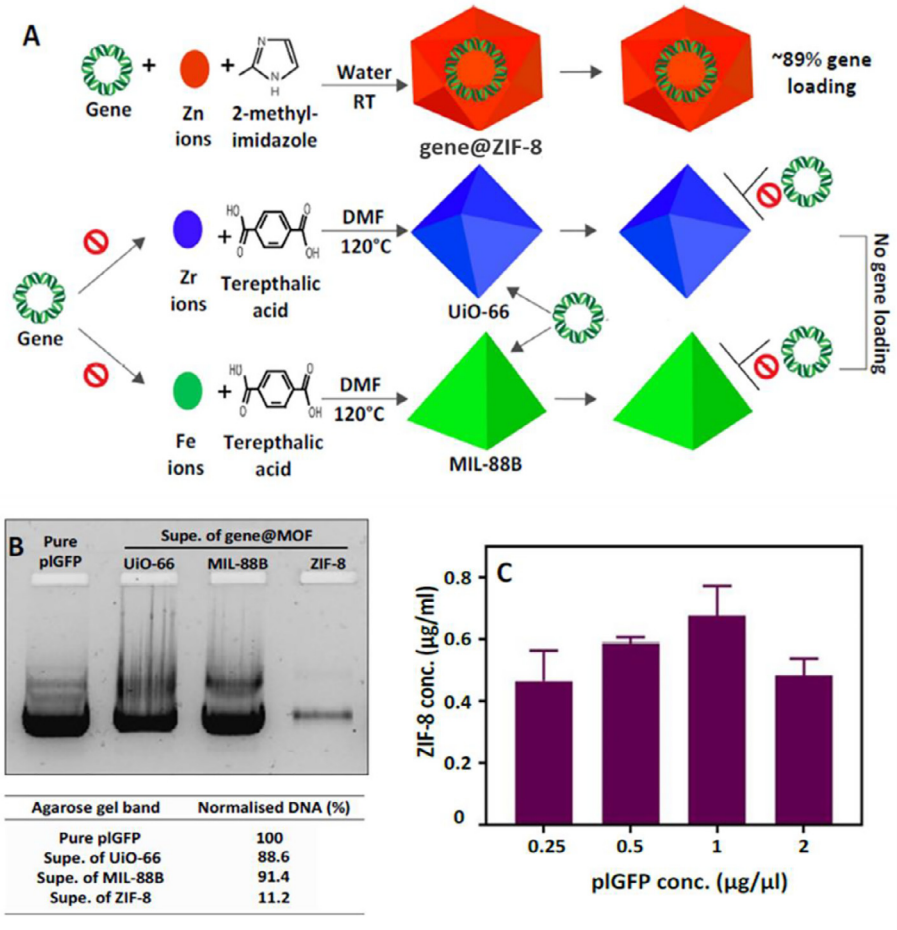

Agarose gel band	Normalised DNA (%)
Pure pIGFP	100
Supe. of UiO-66	88.6
Supe. of MIL-88B	91.4
Supe. of ZIF-8	11.2

Fig. 3. Gene loading. (A) Proposed schematic for gene@MOF synthesis; (B) Gel electrophoresis to visualise and quantify gene amounts remaining in the supernatant; and (C) ICP-MS to determine ZIF-8 quantities for respective amounts of pIGFP used [N=3].

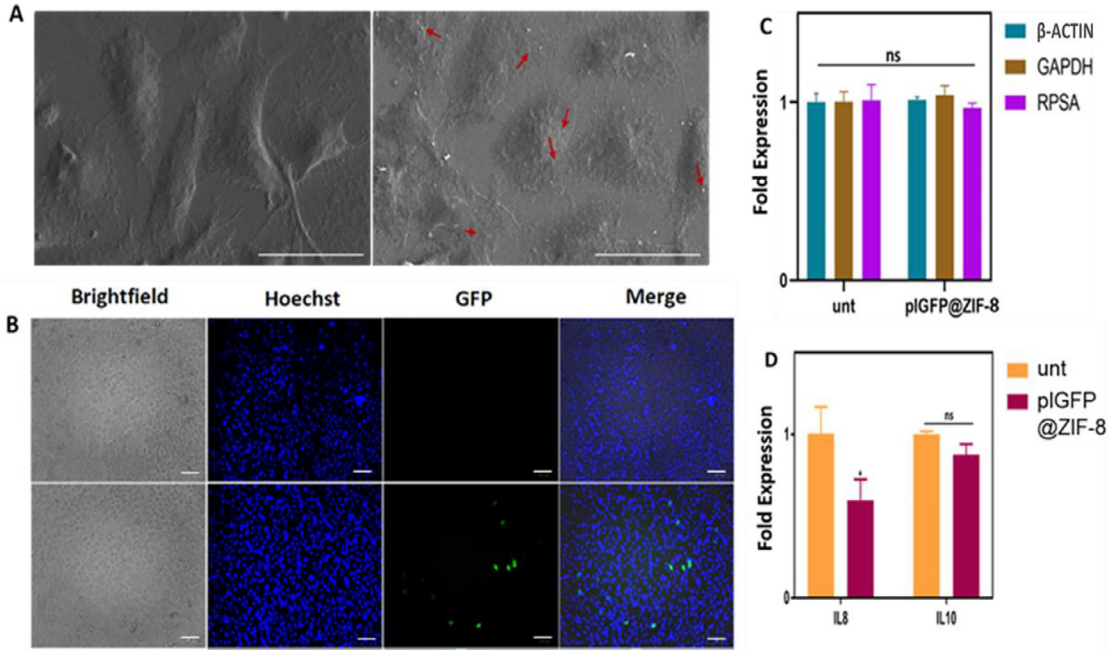

Fig. 4. Gene loading, delivery and cellular impact – (A) SEM imaging to visualize pIGFP@ZIF-8 treatment (right) compared to untreated PC3 cells (left). Red arrows indicate pIGFP@ZIF-8 particles. Scale bars correspond to 40 μm. (B) Fluorescence microscopy images of PC3 cells transfected with growth media (untreated control, top panel); and pIGFP@ZIF-8 (bottom panel). A 1 µg pIGFP used for all. Blue – cell population as seen by Hoechst 33,342 nuclear stain. Green – fluorescence due to protein (GFP) expression from pIGFP, scale bar 100 µm. (C) qRT-PCR to quantify impact on housekeeping genes β-ACTIN and GAPDH and cell-line specific upregulated RPSA, and (D) qRT-PCR to quantify immunomodulation of pro- and anti-inflammatory cytokines IL8 and IL10, respectively. $^{*}p < 0.05$, ns – not significant [N=4].

For MIL-88B, a comparison was done with simulated MIL-88B powder XRD spectrum with CSD details as: ONUKAL, Deposition Number 1,485,530; COD: Information card entry 4,107,051 [46]. For ZIF-8, the comparison was done with simulated ZIF-8 powder XRD spectrum with CSD details as: OFERUN, Deposition Number 652,032 [47]. XRD measurements thus confirmed the characteristic peaks of the synthesized MOFs.

The FTIR spectrum of UiO-66 agreed with the UiO-66 spectrum previously reported. The sample exhibited vibrational characteristics typical for UiO-66. Two strong bands at 1396 and 1589 cm^{-1} were assigned to the symmetric and asymmetric stretchings of O–C–O in the carboxylate groups of the terephthalic acid ligand, respectively [48]. At 1665 cm^{-1} is the N–H bending vibration [49]. The band at 1505 cm^{-1} represents the C=C vibration from the aromatic ring [50]. The characteristic peak at 746 cm^{-1} is ascribed to a mixture of the OH and C–H vibrational bendings and the bands at 661, 548, and 484 cm^{-1} are assigned to the μ3-O stretching, Zr(O–C) stretching, and μ3-OH stretchings [49]. The FTIR spectrum of MIL-88B was in agreement with previous reports. The vibration of $Fe_3(\mu 3\text{-}O)$ is seen at 620 cm^{-1} [51]. The peaks due to symmetric and asymmetric C=O vibrations of the organic linkers and that of C–O of the carboxyl group are observed at 1660 cm^{-1} and 1398 cm^{-1}, respectively [52]. The carboxylate groups (COO-) of the ligands were also confirmed by the appearance of a sharp peak at 683 cm^{-1}. The peak around 2900 cm^{-1} can be assigned to the C–H stretching vibration band of the terephthalic acid linker of MIL-88B [53]. These peaks indicated that the MOFs were successfully synthesized [54]. The FTIR spectrum of ZIF-8 was in agreement with previous reports [40]. The adsorption bands at 2928 cm^{-1} are related to the stretching mode of C–H from the aromatic ring and the aliphatic chain in 2mIM [55]. The observed peaks in the domain of 1350–1550 cm^{-1} are associated with the vibration of the entire ring and the CN stretch emerged at 1584 cm^{-1}. The wavenumber region between 1350 and 950 cm^{-1} shows various bands allocated to the in-plane bending of the ring whereas those observed below 800 cm^{-1} are attributed to the out-of-plane bending. The characteristic peaks of ZIF-8 is in agreement with the reported data [56]. FTIR and UV–vis absorbence spectroscopy further verified the synthesized MOFs where the spectra were in good agreement with reported spectra (Fig. 1G-I and S1). However, UV–Vis for DNA quantification loaded in gene@MOF was insufficient, likely due to inference from intact MOFs or MOF impurities that can interfere and absorb light at wavelengths typically used for DNA detection (260 nm).

4.2. Cytotoxicity

The critical requirement for MOFs to act as successful gene delivery systems is establishing their cytotoxicity. Water washed ZIF-8 complexed with nucleic acids (NA@ZIF-8) has been used for cellular delivery [17]. ZIF-8 has been reported to be toxic from concentrations of 100 μg/ml, followed by lesser toxicity seen by Zr-based MOFs like UiO-66 [13,57]. For Fe-based MOFs like MILs, concentrations up to 80 μg/ml have been reported to be safe [57,58]. The results from cytotoxicity evaluation using MTT assays indicated a progressive decrease in viability with increasing MOF concentrations (Fig. 2). At lower concentrations of up to 25 μg/ml, no significant toxicity was observed for any of the three MOFs, with viability above 80% for all. At higher concentrations, all three MOFs showed similar trends of significantly reduced viability with no significant difference when compared between the MOFs, while retaining good viability at lower concentrations. Thus, cytotoxicity alone was insufficient for selecting the ideal MOF out of UiO-66, MIL-88B and ZIF-8 for gene delivery.

4.3. Gene loading potential: selection of ZIF-8

For assessing gene loading potential, a 6549 basepair plasmid expressing (plGFP) was used. A plasmid is a DNA molecule carrying intact genes that are expressed to proteins in mammalian cells following transfection [34]. Optimal plGFP amounts [36] were used for loading genes onto the MOFs to synthesize gene@MOFs viz. gene@UiO-66, gene@MIL-88B and gene@ZIF-8 washed in water [17] (Fig. 3A, B). It was only in the case of gene@ZIF-8 that ca. 11% of the loaded plGFP remained with the supernatant; indicating nearly 90% of the gene was associated with the ZIF-8 pellet. Hence, gel electrophoresis results provided the basis for indicating the preferential use of ZIF-8. In addition, smeared bands of DNA are seen in the supernatants of MIL-88B and UiO-66, but not in the supernatant of ZIF-8. Smeared bands can be a result of DNA degradation or the presence of contaminants [59]. As pure plGFP shows a band typical of pure plasmid DNA [60], it is likely that smears in the bands associated with UiO-66 and MIL-88B supernatants arose due to the presence of respective MOF precursor contaminants that caused partial degradation of the associated gene. However, the supernatant of ZIF-8 shows a distinct single band free of any smears which is similar to reports of plasmid DNA bands obtained from another magnetic nanoparticle/plGFP formulation [61].

Thus, not only did plGFP fail to associate sufficiently with UiO-66 and MIL-88B, but also gave degraded DNA smears. Limitations of synthesis conditions were another critical step in gene loading. As synthesis conditions of high temperatures (120 °C) and harsh solvents (DMF) are well known to cause complete degradation of DNA [62], UiO-66 and MIL-88B required the gene to be loaded post-synthesis. Thus, ZIF-8 allowed in-situ synthesis due to having aqueous and physiologically favourable room temperature synthesis routes that do not cause DNA degradation. Furthermore, as the gene was introduced to UiO-66 and MIL-88B post-synthesis, the plasmid was unable to load onto the MOF particles. The narrowest pore size that a plasmid can penetrate is reported to be 10 nm [63]. The average pore sizes of UiO-66 and MIL-88B are reported to be 0.5–0.7 nm [52,64-66]. Due to an order of magnitude difference in sizes, it is expected that the plasmid remained in suspension without being loaded onto the MOFs (Fig. 3B). The presence of unreacted precursors in the supernatant could further account for undesirable interaction with DNA, resulting in a smeared band on the agarose gels. However, in the case of Zn-MOFs, the gene could be added in-situ with the reaction precursors at the time of synthesis. Electrostatic interactions between zinc ions and the phosphate backbone of DNA could be a driving force for seeding the MOF structure, with the gene becoming a defect in the MOF scaffold and thus allowing for simultaneous gene loading along with assembly, formation and growth (Fig. 3A).

4.4. Evaluation and visualisation of gene loading in gene@ZIF-8

The maximum amount of gene@ZIF-8 was quantified to be 0.65 μg/ml. Thus, the highest amount of ZIF-8 in gene@ZIF-8 fell well below the cytotoxicity-inducing concentration i.e. 50 μg/ml. Furthermore, cells treated with plGFP@ZIF-8 showed no changes in morphology as compared to untreated controls (Fig. 4A-B). When the cells take up plGFP, the gene is transcribed and translated to express the protein product which is called (GFP). GFP can be detected by fluorescence microscopy. Thus, gene expression of plGFP could be gradually visualized 96 hours post-treatment (Fig. 4B). Viability was retained similar to untreated control cells up to 96 hours, as can be seen from brightfield and Hoechst-stained images. Brightfield images show no damage to cell morphology. Hoechst is a nuclear dye that stains the nucleus and shows no significant changes to cell population. Green fluorescence is detected due to presence of green fluorescence protein (GFP) and, importantly, shows the successful delivery of plGFP by plGFP@ZIF-8. No green fluorescence was seen in cells treated with plGFP@UiO-66 or plGFP@MIL-88B (Fig. S2), confirming the lack of GFP expression due to ineffective gene loading as seen from Fig. 3B.

4.5. Impact of gene@ZIF-8 on constitutive gene expression

Despite its non-toxic nature, introduction of foreign materials to the cellular environment can have a profound impact on their physiology,

metabolism and constitutive architecture. The impact on endogenous physiology was assessed by analysing gene expression levels of two housekeeping markers (β-ACTIN and GAPDH), and a cancer metabolic marker RPSA (Fig. 4C). No significant difference in the expression levels supported the neutrality of the delivery system itself. B-ACTIN expression is responsible for maintaining the cytoskeleton; it is a critical player in the cytoplasm as well as the nucleus and regulates neuronal reprogramming [67]. As seen from the PCR results, the ZIF based MOF delivery system does not disrupt the major biochemical pathways of β-ACTIN expression. Similarly, GAPDH expression levels, critical for diverse functionalities including glycolysis, metabolism, homoeostasis, transcription, post translational modifications and protein interactions [23], also remains unchanged. RPSA, a non-housekeeping gene that is implicated in several protein, viral and bacterial pathologies, and specifically upregulated in aggressive tumors such as advanced prostate cancer [26], also does not undergo any significant change in expression upon the MOF treatment.

4.6. Immunomodulatory impact of gene@ZIF-8

Introduction of novel materials to the cellular environment incites the immune system to respond to the foreign substance. The response is a cumulation of multiple signals leading to immuno-suppression or overstimulation. Hence, any new material that interacts with biological entities must be assessed for their immunotoxicity [68]. To get a complete understanding of impact on the immune system, MOF interaction with the innate and adaptive immune systems, including antibodies, WBCs, the entire complement system as well as the main organs involved need to be studied along with the assessment of immunosuppression or immunostimulation. Such studies for nanomaterials are still under investigation and far from thoroughly understood [68,69]. Thus, a comprehensive immunomodulatory impact requires proper and detailed research beyond the scope of the current report. In order to initiate such necessary studies, impact was assessed on two well-known cytokines (anti and pro-inflammatory) routinely used as tools to study immune responses: anti- and proinflammatory cytokines IL10 and IL8, respectively. Cytokines are essential components that mediate immune response, and are biomarkers for undesirable immune response to engineered biomaterials [30]. Gene expression levels of IL10 and IL8 were quantitated using RT-PCR. No significant over-expression of the cytokines was recorded. An over expression of cytokines in response to treatment is a marker for toxicity, adverse reactions, efficiency and low therapeutic potential [30]. The absence of over expression indicates the lack of negative or undesirable immune response from the MOF delivery system. The suppression of the inflammation-promoting cytokine IL8 was also significant, as was the lack of significant changes to the anti-inflammatory cytokine IL10. IL8 attracts and activates neutrophils, the “first cellular line of defence” to inflammatory regions. Suppression of inflammation allows the MOF delivery system to evade immunostimulation/immunotoxicity. The expression of IL10 demonstrates no significant changes. This is critical as dysregulation of IL10 is associated with an increase in a host of immunopathological responses [32]. Thus, taken together with its non-cytotoxic nature along with the lack of changes to constitutive cellular architecture, the role of gene@ZIF-8 as a neutral non-viral gene delivery agent is further demonstrated.

5. Conclusion

In summary, for biomedical applications of gene therapy, ZIF-based nanomaterial of the MOF subtype is advantageous over UiO-66 and MIL-88B for its potential applications in gene delivery due to the following factors – a. Rapid in-situ synthesis under physiological conditions, b. Successful loading of the gene, c. Low concentration of ZIF-8 is required for gene@ZIF-8 synthesis, and d. Neutral delivery system. In addition, suppression of pro-inflammatory cytokine IL8 along with no significant changes to anti-inflammatory cytokine IL10 pointed towards a lack of immunotoxicity of gene@ZIF-8. The work carried out provides new insight into important considerations before other MOFs can be assessed for gene delivery applications. Explorations on the design of novel MOFs outside of UiOs, MILs and ZIFs could be considered to address the above factors. Though organic solvent washed ZIF-8 has been used for in vitro drug delivery, water washing of gene@ZIF-8 in place of such solvents appears to favour gene delivery; however, physical, chemical and biochemical understandings of this is still considerably nascent and calls for further research. This study opens the focus to critical factors that must be considered for MOFs to be successful for gene delivery-based therapeutics.

Data availability statement

The raw/processed data required to reproduce these findings cannot be shared at this time as the data also forms part of an ongoing study.

Declaration of Competing Interest

The authors declare that they have no known competing financial interests or personal relationships that could have appeared to influence the work reported in this paper.

CRediT authorship contribution statement

A. Poddar: Writing – original draft, Methodology, Investigation, Visualization, Formal analysis. **S. Pyreddy:** Investigation, Validation, Data curation, Writing – review & editing. **S.A. Polash:** Investigation, Validation, Data curation, Writing – review & editing. **C.M. Doherty:** Writing – review & editing, Funding acquisition. **R. Shukla:** Conceptualization, Supervision, Visualization, Project administration, Writing – review & editing, Funding acquisition.

Acknowledgements

A.P. acknowledges joint RMIT-CSIRO PhD scholarship and funding provided by Australian Nanotechnology Network through OTF scheme. S.P. acknowledges Research Training Program (RTP) stipend scholarship (RSS) funded by the Australian Government. S.A.P. acknowledge RMIT Research Stipend Scholarship (RRSS) PhD scholarship. R.S. acknowledges Ian Potter Foundation in establishing Sir Ian Potter NanoBioSensing Facility and the support of ERASMUS program. RMIT Micro Nano Research (MNRF) and Microscopy & Microanalysis (RMMF) facilities are acknowledged for technical assistance.

Supplementary materials

Supplementary material associated with this article can be found, in the online version, at doi:10.1016/j.bbiosy.2022.100065.

References

[1] Gangu KK, et al. A review on contemporary Metal–Organic Framework materials. Inorg Chim Acta 2016;446:61–74.
[2] Wang C, Liu D, Lin W. Metal–organic frameworks as a tunable platform for designing functional molecular materials. J Am Chem Soc 2013;135(36):13222–34.
[3] Yang, J. and Y.-W. Yang, Metal–Organic Frameworks for Biomedical Applications. 2020. 16(10): p. 1906846.
[4] Tian H, et al. Cu-MOF chemodynamic nanoplatform via modulating glutathione and H(2)O(2) in tumor microenvironment for amplified cancer therapy. J Colloid Interface Sci 2021;587:358–66.
[5] Cavka JH, et al. A new zirconium inorganic building brick forming metal organic frameworks with exceptional stability. J Am Chem Soc 2008;130(42):13850–1.
[6] Surblé S, et al. A new isoreticular class of metal-organic-frameworks with the MIL-88 topology. Chem Commun 2006(3):284–6.
[7] Park, K.S., et al., Exceptional chemical and thermal stability of zeolitic imidazolate frameworks. 2006. 103(27): p. 10186–10191.
[8] He C, et al. Nanoscale metal-organic frameworks for the co-delivery of cisplatin and pooled siRNAs to enhance therapeutic efficacy in drug-resistant ovarian cancer cells. J Am Chem Soc 2014;136(14):5181–4.

[9] Zhu X, et al. Inherent anchorages in UiO-66 nanoparticles for efficient capture of alendronate and its mediated release. Chem Commun 2014;50(63):8779–82.
[10] Horcajada P, et al. Porous metal–organic-framework nanoscale carriers as a potential platform for drug delivery and imaging. Nat Mater 2010;9(2):172–8.
[11] Liu YL, et al. A nanosized metal–organic framework of Fe-MIL-88NH2 as a novel peroxidase mimic used for colorimetric detection of glucose. Analyst 2013;138(16):4526–31.
[12] Astria E, et al. Carbohydrates@MOFs. Mater Horiz 2019.
[13] Hoop M, et al. Biocompatibility characteristics of the metal organic framework ZIF-8 for therapeutical applications. Appl Mater Today 2018;11:13–21.
[14] Gao L, et al. Recent advancement of imidazolate framework (ZIF-8) based nanoformulations for synergistic tumor therapy. Nanoscale 2019;11(44):21030–45.
[15] Spitsyna AS, et al. Stability of ZIF-8 nanoparticles in most common cell culture media. Molecules 2022;27(10):3240.
[16] Poryvaev AS, et al. Guest leakage from ZIF-8 particles under drug delivery conditions: quantitative characterization and guest-induced framework stabilization. J Phys Chem C 2021;125(28):15606–13.
[17] Friedmann T. A brief history of gene therapy. Nat Genet 1992;2(2):93–8.
[18] Wang Z, et al. Organelle-specific triggered release of immunostimulatory oligonucleotides from intrinsically coordinated DNA–metal–organic frameworks with soluble exoskeleton. J Am Chem Soc 2017;139(44):15784–91.
[19] Wang S, et al. General and Direct Method for Preparing Oligonucleotide–Functionalized Metal–Organic Framework Nanoparticles. J Am Chem Soc 2017;139(29):9827–30.
[20] Poddar A, et al. Encapsulation, visualization and expression of genes with biomimetically mineralized zeolitic imidazolate framework-8 (ZIF-8). Small 2019;15(36):1902268.
[21] Poddar A, et al. A novel gene delivery approach using metal organic frameworks in human islet-derived progenitor cells. Methods Mol Biol 2019:81–91 **2029**.
[22] Poddar A, et al. ZIF-C for targeted RNA interference and CRISPR/Cas9 based gene editing in prostate cancer. Chem Commun 2020.
[23] Tristan C, et al. The diverse functions of GAPDH: views from different subcellular compartments. Cell Signalling 2011;23(2):317–23.
[24] Lazarev VF, Guzhova IV, Margulis BA. Glyceraldehyde-3-phosphate dehydrogenase is a multifaceted therapeutic target. Pharmaceutics 2020;12(5):416.
[25] Perrin BJ, Ervasti JM. The actin gene family: function follows isoform. Cytoskeleton (Hoboken, N.J.) 2010;67(10):630–4.
[26] Bunnell, T.M., et al., β-Actin specifically controls cell growth, migration, and the G-actin pool. 2011. 22(21): p. 4047–4058.
[27] DiGiacomo V, Meruelo D. Looking into laminin receptor: critical discussion regarding the non-integrin 37/67-kDa laminin receptor/RPSA protein. Biol Rev Camb Philos Soc 2016;91(2):288–310.
[28] Roy JG, McElhaney JE, Verschoor CP. Reliable reference genes for the quantification of mRNA in human T-cells and PBMCs stimulated with live influenza virus. BMC Immunology 2020;21(1):4.
[29] Zhang, B., et al., β-Actin: not a suitable internal control of hepatic fibrosis caused by Schistosoma japonicum. 2019. 10(66).
[30] Elsabahy M, Wooley KL. Cytokines as biomarkers of nanoparticle immunotoxicity. Chem Soc Rev 2013;42(12):5552–76.
[31] Bickel M. The role of interleukin-8 in inflammation and mechanisms of regulation. J Periodontol 1993;64(5 Suppl):456–60.
[32] Iyer SS, Cheng G. Role of interleukin 10 transcriptional regulation in inflammation and autoimmune disease. Crit Rev Immunol 2012;32(1):23–63.
[33] Kumar S, et al. Association between pro-(IL-8) and anti-inflammatory (IL-10) cytokine variants and their serum levels and H. pylori-related gastric carcinogenesis in northern India. Meta Gene 2015;6:9–16.
[34] Kroll J, et al. Plasmid addiction systems: perspectives and applications in biotechnology. Microb Biotechnol 2010;3(6):634–57.
[35] Thomas, C.M. and D. Summers, *Bacterial Plasmids*, in *eLS*. 2001, John Wiley & Sons, Ltd.
[36] Li Y, et al. Encapsulation of plasmid DNA by nanoscale metal–organic frameworks for efficient gene transportation and expression. Adv Mater 2019;31(29):1901570.
[37] Moberly JG, Bernards MT, Waynant KV. Key features and updates for Origin 2018. J Cheminformatics 2018;10(1):5.
[38] Li B, et al. Ferrocene particles incorporated into Zr-based metal–organic frameworks for selective phenol hydroxylation to dihydroxybenzenes. RSC Adv 2017;7:38691–8.
[39] Yi X, et al. NH2–MIL-88B–Fe for electrocatalytic N2 fixation to NH3 with high Faradaic efficiency under ambient conditions in neutral electrolyte. J Mater Sci 2020:55.
[40] Liang K, et al. Biomimetic mineralization of metal-organic frameworks as protective coatings for biomacromolecules. Nat Commun 2015;6(1):7240.
[41] Schindelin J, et al. Fiji: an open-source platform for biological-image analysis. Nat Methods 2012;9(7):676–82.
[42] Zahmakiran M. Iridium nanoparticles stabilized by metal organic frameworks (IrNPs@ZIF-8): synthesis, structural properties and catalytic performance. Dalton Trans 2012;41(41):12690–6.
[43] Chen X, et al. MOF nanoparticles with encapsulated autophagy inhibitor in controlled drug delivery system for antitumor. ACS Appl Mater Interfaces 2018;10(3):2328–37.
[44] Hardikar AA, Farr RJ, Joglekar MV. Circulating microRNAs: understanding the limits for quantitative measurement by real-time PCR. J Am Heart Assoc 2014;3(1):e000792.
[45] Øien S, et al. Detailed structure analysis of atomic positions and defects in zirconium metal–organic frameworks. Cryst Growth Des 2014;14(11):5370–2.
[46] Horcajada P, et al. How linker's modification controls swelling properties of highly flexible Iron(III) dicarboxylates MIL-88. J Am Chem Soc 2011;133(44):17839–47.
[47] Katsenis AD, et al. In situ X-ray diffraction monitoring of a mechanochemical reaction reveals a unique topology metal-organic framework. Nat Commun 2015;6:6662.
[48] Valenzano L, et al. Disclosing the complex structure of UiO-66 metal organic framework: a synergic combination of experiment and theory. Chem Mater 2011;23(7):1700–18.
[49] DeCoste JB, et al. The effect of water adsorption on the structure of the carboxylate containing metal–organic frameworks Cu-BTC, Mg-MOF-74, and UiO-66. J Mater Chem A 2013;1(38):11922–32.
[50] DeCoste JB, et al. Stability and degradation mechanisms of metal–organic frameworks containing the Zr6O4(OH)4 secondary building unit. J Mater Chem A 2013;1(18):5642–50.
[51] Yazdanbakhsh M, et al. Synthesis, X-ray crystal structure and spectroscopic characterization of heterotrinuclear oxo-centered complex [Fe2NiO(CH3CH2COO)6(H2O)3]. J Mol Struct 2010;982(1):176–80.
[52] Vuong G-T, Pham M-H, Do T-O. Synthesis and engineering porosity of a mixed metal Fe2Ni MIL-88B metal–organic framework. Dalton Trans 2013;42(2):550–7.
[53] Nandiyanto, A.B.D., R. Oktiani, and R. Ragadhita, *How to read and interpret FTIR spectroscope of organic material.* 2019. 4(1): p. 22.
[54] Ma, M., et al., Iron metal–organic frameworks MIL-88B and NH2-MIL-88B for the loading and delivery of the gasotransmitter carbon monoxide. 2013. 19(21): p. 6785–6790.
[55] Wu C, et al. *Unveiling the thermolysis natures of ZIF-8 and ZIF-67 by employing* in situ *structural characterization studies*. Phys Chem Chem Phys 2019;21(32):17571–7.
[56] Yang X, et al. Synthesis of ZnO/ZIF-8 hybrid photocatalysts derived from ZIF-8 with enhanced photocatalytic activity. Inorg Chem Front 2018;5(3):687–93.
[57] Tamames-Tabar C, et al. Cytotoxicity of nanoscaled metal–organic frameworks. J Mater Chem B 2014;2(3):262–71.
[58] Chen G, et al. In vitro toxicity study of a porous iron(III) metal–organic framework. Molecules 2019;24(7).
[59] Stellwagen NC. Electrophoresis of DNA in agarose gels, polyacrylamide gels and in free solution. Electrophoresis 2009;30(Suppl 1):S188–95 **Suppl 1**.
[60] Meyers JA, et al. Simple agarose gel electrophoretic method for the identification and characterization of plasmid deoxyribonucleic acid. J Bacteriol 1976;127(3):1529–37.
[61] Cui J, et al. Application of PEI-modified magnetic nanoparticles as gene transfer vector for the genetic modification of animals. Adv Mater Sci Eng 2012:764521 2012.
[62] Karni M, et al. Thermal degradation of DNA. DNA Cell Biol 2013;32(6):298–301.
[63] Arkhangelsky E, et al. Kinetics and mechanism of plasmid DNA penetration through nanopores. J Membr Sci 2011;371(1):45–51.
[64] Idrees KB, et al. Tailoring pore aperture and structural defects in zirconium-based metal–organic frameworks for krypton/xenon separation. Chem Mater 2020;32(9):3776–82.
[65] Wu H, Yildirim T, Zhou W. Exceptional mechanical stability of highly porous zirconium metal–organic framework UiO-66 and its important implications. J Phys Chem Lett 2013;4(6):925–30.
[66] He J, et al. Highly efficient Fenton and enzyme-mimetic activities of NH2-MIL-88B(Fe) metal organic framework for methylene blue degradation. Sci Rep 2018;8(1):5159.
[67] Gjorgjieva T, et al. Loss of β-actin leads to accelerated mineralization and dysregulation of osteoblast-differentiation genes during osteogenic reprogramming. Adv Sci 2020;7(23):2002261.
[68] Zolnik BS, et al. Nanoparticles and the immune system. Endocrinology 2010;151(2):458–65.
[69] Dwivedi PD, et al. Impact of nanoparticles on the immune system. J Biomed Nanotechnol 2011;7(1):193–4.